Imaging complex model catalysts in action: From surface science towards industrial practice using high-pressure scanning tunneling microscopy

Mom, R.V.

Chapter 3

In situ observations of an active MoS_2 hydrodesulfurization model catalyst

The hydrodesulfurization process is used to remove harmful sulfur from oil to produce clean hydrocarbons. Using high-pressure scanning tunneling microscopy, we provide the first direct observations of a MoS_2 hydrodesulfurization catalyst under reaction conditions. We show that the active edge sites of the catalyst nanoislands adapt their sulfur, hydrogen, and hydrocarbon coverages depending on the gas environment. By comparing these observations to density functional theory calculations, we propose that the dominant edge structure during the desulfurization of CH_3SH contains a mixture of adsorbed sulfur and CH_3SH. Counterintuitively, the edge sulfur content is reduced by the presence of CH_3SH. In contrast, our theoretical analysis shows that a subtle lowering of the C-S bond-breaking barrier would result in sulfur deposition that is able to push the edge sulfur coverage far above its equilibrium value.

3.1 Introduction

The hydrodesulfurization (HDS) process is used to remove environmentally harmful sulfur from ~2.500 million tons of oil annually[1]. Thus, it is an essential step in the production of clean fuels. To accomplish the removal of sulfur, the oil is mixed with hydrogen at a pressure between 5 bar and 160 bar, with the temperature between 533 K and 653 K, producing H_2S and clean hydrocarbons[2].

MoS_2-based catalysts are widely used to drive the HDS reaction owing to their high activity, stability and low cost[2]. While research into these catalysts started as early as the 1920's[3], the atomic-scale mechanism of the reaction is still under debate. Ex situ microscopy data showed that MoS_2 is present as nanoislands that consist of one or more layers of an S-Mo-S sandwich[4–10]. The edges of the islands serve as active sites during catalysis[11–14]. Hence, mechanistic understanding of the HDS process requires detailed knowledge of the properties of the edge sites.

In most cases, the MoS_2 islands exhibit a high degree of crystallinity, resulting in island shapes close to the thermodynamically favored truncated triangle[4–8,15,16]. Consequently, two types of edge termination are mainly observed, usually referred to as the Mo edge and the S edge, with the Mo edge being dominant. *Ab initio* thermodynamics calculations predict that the sulfur coverage on both edge structures depends on the gas environment[15,17–19]. The essential element is the balance between the chemical potentials of hydrogen and sulfur atoms in the gas phase. In a sulfur-rich feed, two S edge atoms per Mo edge atom (100% coverage) are predicted. Excess hydrogen can lower this number, in the limit of pure H_2 even to zero (0% coverage).

Experimental studies in several gas environments confirmed that the edge sulfur coverage varies, depending on the balance between hydrogen and sulfur containing species in the feed[15,20,21]. However, it remains extremely challenging to study a minority species such as edge atoms under *operando* conditions. As a result, a conclusive determination of the active site structure during HDS has so far not been achieved.

Here, we present the first direct observations of the active MoS_2 edge structure under reaction conditions. Using a special-purpose high-pressure scanning tunneling microscope (STM), we have obtained atomically resolved images evidencing a mixed hydrocarbon-sulfur edge structure during the desulfurization of CH_3SH on a model catalyst. We explain the observations by comparing the STM images with density functional theory (DFT) calculations, also taking into account the role of the reaction kinetics in determining the active site structure.

3.2 Results and discussion

The combination of high pressures of corrosive gases and high temperature provides a challenging environment for STM experiments. To meet this challenge, we have used the ReactorSTM previously developed in our group[22]. At the heart of this system is a 0.5 ml flow reactor containing the STM tip. The reactor walls are defined by a cap placed inside the scan piezo, the catalyst sample, the STM body, and polymer seals in between these elements. Gas capillaries drilled in the STM body provide a connection to a gas supply system that controls the composition, flow, and pressure of the gases in the flow reactor.

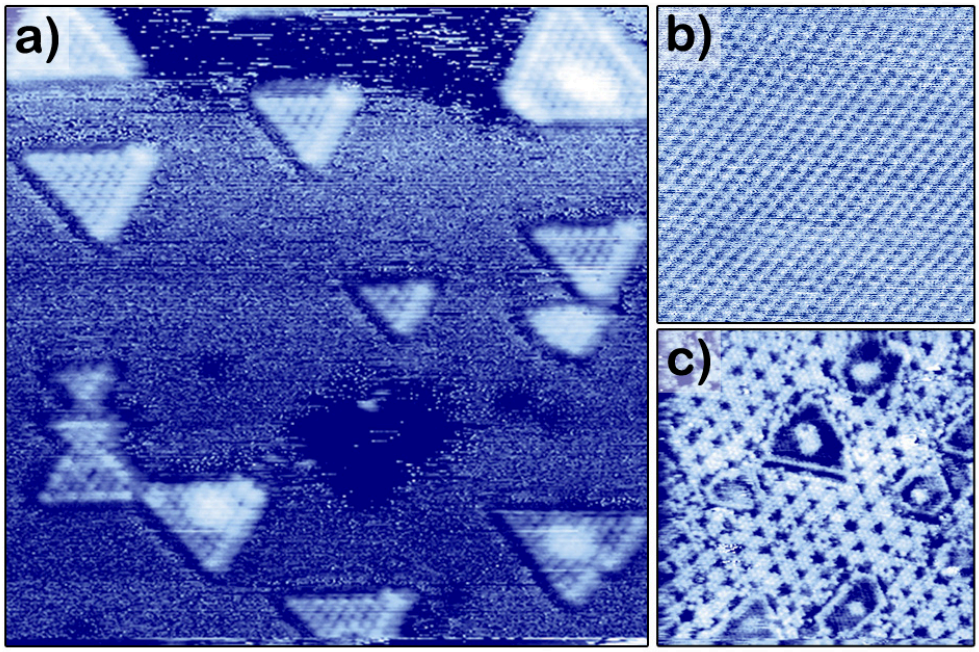

Figure 3.1: STM images of a MoS_2/Au(111) model catalyst and its stability under desulfurization conditions. a) Catalyst after preparation in UHV. 16 x 16 nm^2, U_{bias} = -0.3 V, I_t = 320 pA. b) Clean Au surface imaged in 1 bar CH_3SH at 523 K, showing the (1x1) Au lattice. 6 x 6 nm^2, U_{bias} = -0.3 V, I_t = 550 pA. c) MoS_2/Au(111) after 1 day in 1 bar of a 1:9 CH_3SH/H_2 mixture, showing a sulfur overlayer on the Au(111) substrate. 20 x 20 nm^2, U_{bias} = -0.3 V, I_t = 645 pA.

To mimic realistic industrial conditions, the pressure can be raised up to 1 bar, while the sample is heated up to 573 K using a filament located on the backside of the sample. A key element in the design is that the scan piezo is not in contact with the gases in the reactor. This geometry, in combination with a careful choice of chemically resistant materials, allows for the use of highly corrosive gases such as H_2S at elevated temperatures. The use of PtIr tips prevents tip degradation during the measurements, albeit that frequent changes in imaging quality cannot be avoided. To combine the

high-pressure experiments with more traditional ultrahigh vacuum (UHV) surface preparation and characterization techniques, the flow reactor can be opened and closed inside a UHV system, which contains a.o. an ion gun, an evaporation source, and an X-ray photoelectron spectroscopy apparatus.

As a first step, we established a suitable model catalyst; one that is conductive to allow for STM measurements and stable under HDS conditions. Following the successful recipe of the Århus group[4,15], we synthesized MoS_2 particles on a Au(111) substrate (see Methods section), yielding crystalline islands with a predominantly triangular shape (see Figure 3.1a). These islands were shown to nearly exclusively expose the Mo edge[15], which we will focus on hereafter.

The stability of the model catalyst during HDS depends on the chosen conditions. To allow for unambiguous identification of edge structures in STM, we chose the simple CH_3SH molecule as our organosulfur compound to be desulfurized. Like all thiols, CH_3SH readily adsorbs on gold surfaces[23]. However, at the temperature of our catalytic experiments (523 K), only the (1x1) Au lattice is imaged, even in 1 bar CH_3SH (see Figure 3.1b). Over time, a sulfur overlayer is formed, resulting from decomposition of CH_3SH or H_2S. As long as H_2S is not added to the reactor feed, this process requires hours, making it too slow to interfere with the HDS catalysis on the MoS_2 particles through sulfur spillover. However, the 'encapsulation' of the MoS_2 particles by the sulfur overlayer on the Au substrate, depicted in Figure 3.1c, could limit the accessibility of the active edge sites. To prevent this, we restricted the duration of our HDS experiments to a few hours, after which a fresh model catalyst was prepared.

As a next step, we characterized the appearance of the fully sulfided MoS_2 edge structure obtained after preparation of the MoS_2 particles in $2x10^{-6}$ mbar pure H_2S. Using DFT calculations, Lauritsen *et al.* [15] identified the resulting edge structure as the 100%S edge, which contains an S dimer on every Mo edge atom. Its appearance in STM images is characterized by a periodicity of one lattice spacing along the edge and by a registry shift of half a lattice spacing in the apparent position of the edge atoms with respect to those on the basal plane. This shift is highlighted by the yellow line in Figure 3.2a. Note from the ball model in Figure 3.2a that the apparent position of the edge atoms in STM deviates from their geometrical position. This is a result of the fact that the electronic states around the Fermi level, which are probed by STM, are mostly located in between the edge atoms (see Figure 3.6a in the Supporting Information).

Our first step towards reaction conditions is to image the model catalyst in high H_2 pressure and at high temperatures. Under these conditions, the appearance of the edge sites changes (see Figure 3.2b), indicating that the edge sites have been reduced. The registry shift of the "edge atoms" with respect to the basal plane atoms that was apparent for the 100%S edge has been removed, while maintaining the periodicity along the edge of one lattice spacing. The structure in Figure 3.2b was not dependent on temperature within the range from 323 K to 523 K probed here. It should be noted

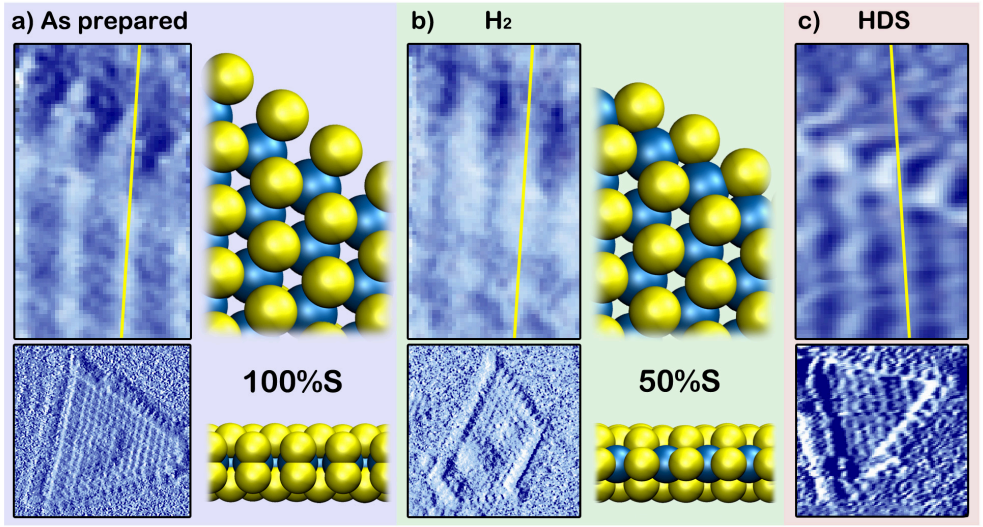

Figure 3.2: MoS_2 edge structure in various gas environments. The bottom panels show the original images, which were differentiated to highlight the atomic contrast. The top panels depict the averaged edge unit cell obtained from the bottom panels. For a) and b), the ball models represent the structures that could directly be identified from comparison to simulated STM images (see Figure 3.6 in the Supporting Information). Blue: Mo, yellow: S. a) Catalyst after preparation in $2x10^{-6}$ mbar H_2S at 723 K, imaged in UHV at room temperature. 6.6 x 6.6 nm^2, U_{bias} = -0.3 V, I_t = 560 pA. b) Catalyst imaged in 1 bar H_2 at 323 K. 6.6 x 6.6 nm^2, U_{bias} = -0.3 V, I_t = 630 pA. c) Catalyst during the desulfurization of CH_3SH in 1 bar 1:9 CH_3SH/H_2 at 523 K. 3.8 x 3.8 nm^2, U_{bias} = -0.3 V, I_t = 400 pA.

however that at elevated temperatures STM may probe a time-averaged structure, which could obscure diffusing S vacancies or adsorbed S and H atoms.

The edge structure without registry shift in Figure 3.2b was also observed after deposition of Mo in H_2S/H_2 mixtures[15] or dimethylsulfide[24]. It was interpreted as the 50%S structure by comparison to simulated STM images. Our STM simulations corroborate this assignment, although hydrogen adsorption cannot be excluded (see Section 3.5 in the Supporting Information). We note that Bruix *et al.* did not find the registry shift between the 100%S and the 50%S edge structures for MoS_2/Au(111) in their STM simulations[21]. However, none of the structures described in their work matches the experimental observations of the reduced edge structure.

Having established our ability to observe changes in the MoS_2 edge structure under high-pressure, high-temperature conditions, we are ready to study our model catalyst in its active form during the desulfurization of CH_3SH. Figure 3.2c shows the structure observed in a 1 bar 1:9 CH_3SH/H_2 mixture at 523 K. Before imaging, the flow reactor was allowed to stabilize for more than 2 hours to ensure a steady state situation. Figure 3.2c shows that the edge structure under hydrodesulfurization conditions has

clearly changed with respect to the structure in pure hydrogen. Based on the apparent registry of the edge atoms, one could assign the structure to an (almost) 100%S-covered edge. An alternative explanation is the formation of CH_3SH adsorption structures.

To enable an unambiguous assignment of the edge structure observed during the hydrodesulfurization of CH_3SH, we consider the thermodynamic and kinetic aspects of the catalytic process using DFT calculations. First, we assess the thermodynamic stability of various edge structures in a gas environment that only consists of H_2 and H_2S. Figure 3.3 depicts the most stable edge structure for Au-supported MoS_2 as a function of $\Delta\mu_S$ and $\Delta\mu_H$. These quantities are directly related to the temperature, the H_2S pressure, and the H_2 pressure through Equations 3.5 and 3.6 in the Methods section. The phase diagram in Figure 3.3 corroborates the observation that the MoS_2 edge structure depends on the gas environment, showing large variations in both S and H coverage. A quantitative comparison to earlier work shows an agreement to within 0.15 eV for the relative stability of the 50%S and 100%S structures[15,18,19] (see Table 3.1 in the Supporting Information). Remarkably however, we find a preference for low-symmetry structures such as 38%S-x%H and 63%S-x%H over a wide range of conditions. These structures were not taken into account in earlier studies and therefore did not show up in the predicted phase diagrams.

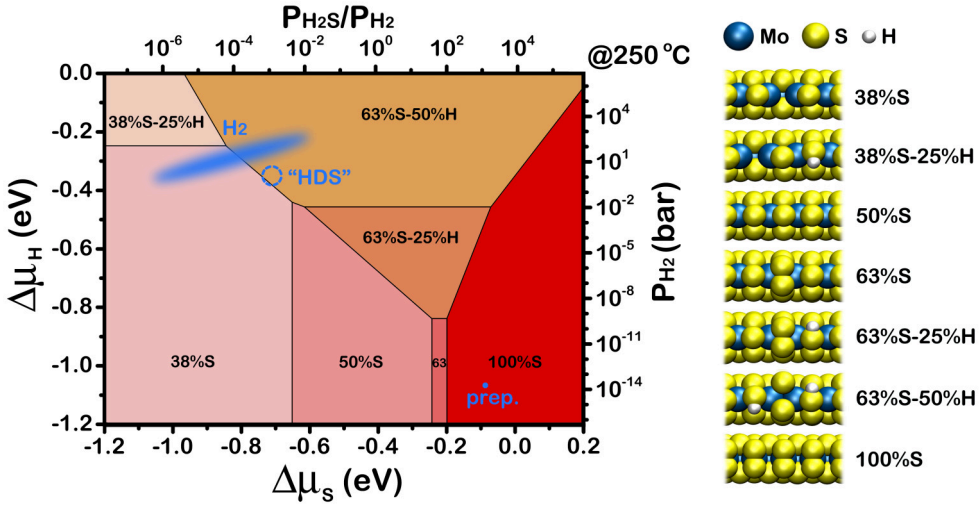

Figure 3.3: *Ab initio* thermodynamics phase diagram of the MoS_2 edge structures in H_2/H_2S mixtures for Au-supported MoS_2. On the axes, $\Delta\mu_S$ and $\Delta\mu_H$ designate the entropic parts of the chemical potentials of S and H atoms in the gas phase, respectively. These are directly related to the temperature, the H_2S pressure, and the H_2 pressure (see Methods section). The experimental conditions during catalyst preparation, in 1 bar hydrogen (assuming 1 ppm H_2S contamination), and during HDS (naïve approximation) are indicated in blue. The ball models represent side views of the structures present in the phase diagram. Note that the edges are periodic in the left-right direction.

The trends of the sulfur and hydrogen coverages in various gas environments can be understood based on the variation in adsorption strength per H or S atom of the various structures. Generally, one expects the adsorption strength per S or H atom to decrease at higher S or H coverage. Hence, higher-coverage structures require a higher chemical potential in order to form. This trend is indeed observed in the phase diagram. However, the 75%S and 88%S structures do not appear. In this coverage range, the registry of the S edge atoms changes with respect to the S atoms on the basal plane, leading to unstable structures with strained bonds. For the hydrogenated phases, 63%S-x%H shows a remarkably large range of stability. An explanation for this comes from the comparison of the 50%S and 63%S structures in Figures 3.2b and 3.3. For the 50%S case, hydrogen adsorption induces buckling of the edge S atoms, implying the presence of compressive stress. The buckling disappears upon the adsorption of a sulfur atom (yielding the 63%S-50%H structure), implying a stabilizing stress relief. For the small particles used in HDS, corner sites may provide similar stress relief. It is therefore not a priori clear whether the 63%S-x%H structures are similarly stable in such more realistic catalysts.

Using equations 3.5 and 3.6 (see Methods section), we have placed the experimental conditions in the phase diagram of Au-supported MoS_2. For the freshly prepared particles, we have used an H_2S pressure of $2x10^{-6}$ mbar H_2S and a temperature of 573 K for the calculation, even though imaging was performed in vacuum at room temperature. We chose these conditions because the edge structure is not capable of changing in vacuum at temperatures below 573 K[15,21]. As expected, the phase diagram indicates the observed 100%S structure to be the most stable under these conditions. For the reduction in 1 bar H_2, we assumed an H_2S contamination level of 1 ppm. Depending on the temperature, the phase diagram indicates an edge coverage of 38%S to 63%S, with hydrogen adsorption on most structures. Again, this is in good agreement with the time-averaged 50%S-50%H structure observed with STM.

To represent the hydrodesulfurization experiment in the phase diagram, we need to assume that the gas environment can be described solely in terms of H_2S and H_2 chemical potentials. This would be the case if the adsorption of hydrocarbons, e.g. CH_3SH, is ignored and the overall HDS reaction is either completely equilibrated or slow with respect to the reactions of H_2 and H_2S with the MoS_2 edges. From mass spectroscopic product analysis, we know that in our case the conversion of CH_3SH is low due to the extremely low number of active sites on our planar model catalyst. Even at an extremely high turnover frequency of 1000 s^{-1} per site, only approximately 1 mbar H_2S would be generated. If we assume this upper limit and ignore CH_3SH adsorption, the chemical potential of sulfur in our HDS experiment is determined by the temperature (523 K), the H_2S pressure ($\sim$0.001 bar) and the H_2 pressure (0.9 bar), as indicated in Figure 3.3. This would lead to a 63%S-50%H structure, which has a slightly higher S coverage than the 50%S-50%H structure predicted in earlier studies for these conditions[15,18]. It should be clear however that the 100%S structure is not a likely candidate for the structure we observe in STM under reaction conditions.

To investigate the possibility of CH_3SH adsorption structures, we calculated the CH_3SH adsorption energy for several edge S and H coverages on Au-supported MoS_2 (see Table 3.2 in the Supporting Information). While CH_3SH can bind in all cases, only the 38%S-25%CH_3SH structure in Figure 3.4 is thermodynamically more stable (ΔG_{form}= -0.08 eV) than the clean 63%S-50%H structure under our reaction conditions (P_{CH3SH} = 0.1 bar, P_{H2S} = ~0.001 bar, P_{H2} = 0.9 bar, 523 K). Hence, if H_2, H_2S, and CH_3SH would equilibrate with our model catalyst, i.e. if the HDS reaction would be slow enough not to affect this thermodynamic equilibrium, the 38%S-25%CH_3SH structure should prevail. For H_2S pressures lower than the upper limit of 1 mbar we, the preference for the 38%S-25%CH_3SH is further increased. Figure 3.4b shows an STM simulation of the 38%S-25%CH_3SH structure. Clearly, the edge atoms appear out of registry with the basal plane S atoms, in agreement with the experimental observations. The irregular appearance in Figure 3.4b will be time-averaged in the STM images at 523 K, because of the fast adsorption/desorption kinetics of CH_3SH (free energy barriers of 0.51 eV and 0.87 eV, respectively).

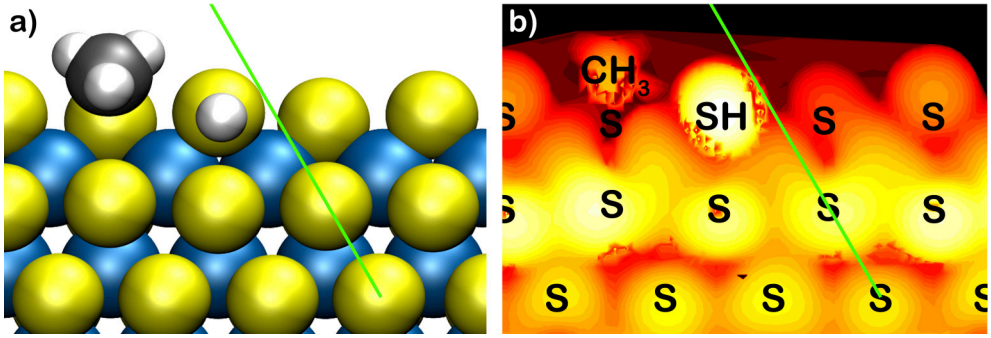

Figure 3.4: Thermodynamically preferred structure under the experimental desulfurization conditions (P_{CH3SH} = 0.1 bar, P_{H2S} = ~0.001 bar, P_{H2} = 0.9 bar, 523 K). The green lines highlight the registry shift of the edge atoms with respect to the basal plane S atoms, which was also observed in the experiment. a) Ball model. b) Simulated STM image for U_s = -0.3 V, using an electron density contour value of $1x10^{-5}$ AU.

Since we have come close to industrial conditions in our HDS experiment, we expect conversion of CH_3SH to CH_4. Hence, the reaction should be in a steady state rather than in the static equilibrium discussed in the previous paragraph. To model how this affects the prevalent edge structure, we computed a reaction network linking a set of reaction intermediates on Au-supported MoS_2 (see Figure 3.5). The catalytic cycles in the network consist of three stages: the conversion of CH_3SH to CH_4, leaving behind a sulfur atom on the MoS_2 edge, the desorption of this sulfur atom as H_2S, and the adsorption of hydrogen. From Figure 3.5, it is clear that the conversion of CH_3SH is essentially a one-way reaction due to its high energy gain. In contrast, the adsorption/desorption steps of H_2, H_2S, and CH_3SH are all reversible.

Putting this in a simple steady state rate equation model we obtain:

$$CH_3SH_{ads} \rightarrow CH_{4(g)} + S_{ads} \tag{3.1}$$

$$S_{ads} + H_{2(g)} + CH_3SH_{(g)} \rightleftharpoons H_2S_{(g)} + CH_3SH_{ads} \tag{3.2}$$

$$\frac{[S_{ads}]}{[CH_3SH_{ads}]} = \frac{k_1 + k_{-2}P_{H_2S}}{k_2 P_{H_2} P_{CH_3SH}} \tag{3.3}$$

Although highly simplified, this model provides some insight into the effect of CH_3SH conversion on the MoS_2 edge structure. When the conversion faces a high barrier, rate constant k_1 will be low. In such a case, the edge structure should be close to the equilibrium of Equation 3.2. In contrast, when the barrier for CH_3SH conversion would be lower than the H_2/H_2S adsorption/desorption barriers, one should expect that adsorbed CH_3SH would be largely replaced by sulfur atoms.

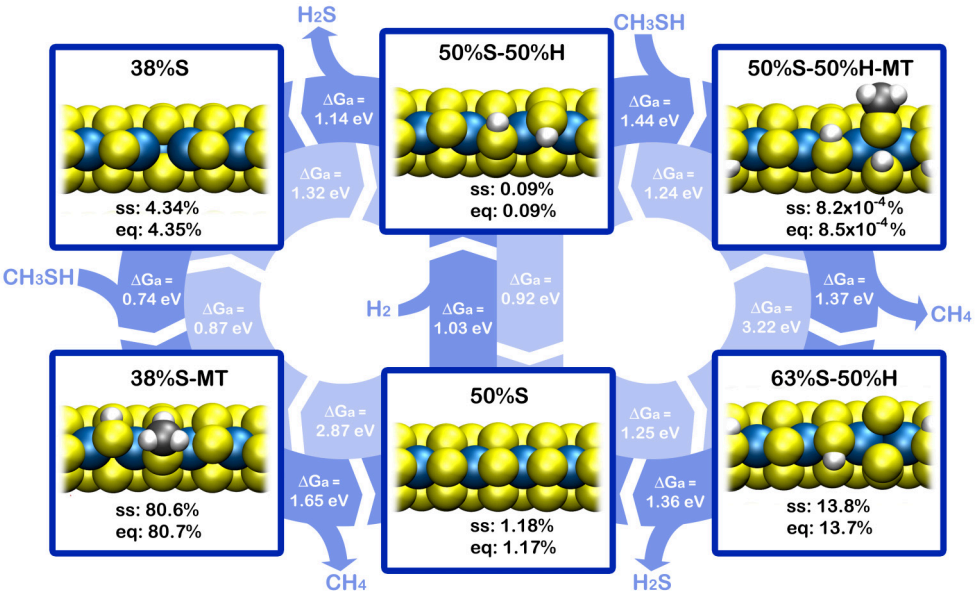

Figure 3.5: Reaction network for CH_3SH desulfurization on MoS_2/Au(111). The activation free energy barriers (ΔG_a) indicated in the arrows were calculated based on the experimental conditions (P_{CH3SH} = 0.1 bar, P_{H2S} = ~0.001 bar, P_{H2} = 0.9 bar, 523 K). The abundances of intermediates in steady state conditions and in an equilibrium where the C-S bond breaking step is disabled are designated by ss and eq, respectively. The steady state concentrations were derived using transition state theory and rate equation modeling (see Methods section). "MT" corresponds to methane thiol.

Figure 3.5 shows that the C-S bond breaking barriers are slightly higher than the H_2S desorption barriers. Because the rate constants have an exponential dependence on the energy barrier, this translates into orders of magnitude difference in rate. Indeed,

when we quantify the abundances of all reaction intermediates (see Methods section), we still find an 80.6% abundance of the 38%S-CH_3SH edge state, compared to 80.7% under equilibrium conditions. Hence it appears that the structure observed in our HDS experiment is the 38%S-CH_3SH edge state.

In a more general view, our theoretical analysis identifies two mechanisms that can steer the MoS_2 edge structure away from its equilibrium with H_2 and H_2S during the HDS reaction. First, the adsorption of organic molecules may favor different edge S and H coverages. In our experiments, this leads to the counterintuitive observation that the edge S content is reduced due to CH_3SH adsorption: the 67%S-50%H structure is favored in the absence of CH_3SH adsorption, whereas the 38%S-25%CH_3SH structure is the most stable one when we do take CH_3SH adsorption into account. This effect is likely also present for industrially important reaction intermediates such as reduced thiophenes, which adsorb strongly[25]. A second mechanism is the deposition of sulfur via C-S bond scission. Although this appears to have only a minor effect in our experiment, subtle changes in the barrier for C-S bond breaking can have major consequences for the average edge structure. For instance, if the C-S barrier in the network in Figure 3.4 were lowered by 0.3 eV, the 63%S-50%H structure would become dominant. Hence, support effects, the presence of defects such as corner sites, and the nature of the hydrocarbons that are desulfurized can all cause large variations in the average structure of MoS_2 under reaction conditions.

3.3 Conclusion

Using a dedicated high-pressure scanning tunneling microscope, we have studied the catalytically active edge structure of MoS_2 nanoparticles on Au(111) in mixtures of H_2, H_2S, and CH_3SH at temperatures up to 523 K. In hydrogen, trace amounts of sulfur in the feed are sufficient to maintain a sulfur coverage of 1 edge S atom per edge Mo atom. Surprisingly, the edge is reduced during the hydrodesulfurization of CH_3SH to accommodate CH_3SH adsorption. Due to the slow C-S bond scission on our model catalyst, the system remains close to an equilibrium state. However, our theoretical analysis indicates that small changes in the reaction rate or the reaction mechanism, which could originate from support effects or from the presence of different hydrocarbons, can have a major influence on the average MoS_2 edge structure. In particular, for highly active MoS_2 catalysts one may expect that sulfur deposition by the conversion of organosulfur compounds increases the edge S coverage under hydrodesulfurization conditions, rather than to decrease it, as was found here. Hence, we conclude that the prevalent structure of the active sites during hydrodesulfurization catalysis on MoS_2 likely depends both on the precise type of catalyst and the nature of the feedstock.

3.4 Methods

3.4.1 Model catalyst preparation

Clean, atomically smooth Au(111) was prepared by cycles of 1 keV Ar^+ bombardment and annealing at 900 K. MoS_2 particles were deposited by evaporation of Mo in $1x10^{-6}$ mbar H_2S, with the Au substrate at 423 K, followed by annealing at 723 K in $2x10^{-6}$ mbar H_2S.

3.4.2 High-pressure experiments.

All gas lines were flushed with argon for at least 30 minutes prior to each experiment. To start the high-pressure exposure, the reactor was slowly pressurized in H_2 and subsequently heated to the desired temperature. For the HDS experiments, CH_3SH was mixed in the reactor feed only after reaching 523 K. In order to minimize the thermal drift in the microscope, the system was allowed an equilibration period of approximately 90 minutes. To cope with the remaining drift, image acquisition times of around 20 seconds per image were employed. As the noise level increased under high-pressure, high-temperature conditions, a 3x3 pixel averaging was applied for clarity.

3.4.3 Theoretical analysis.

All DFT calculations were carried out with the BAND program package[26–30], using the PBE density functional[31], Grimme van der Waals corrections[32], and scalar relativistic corrections. A triple-ζ plus polarization basis set was used for the valence orbitals, while the core orbitals were kept frozen in the same state as in the free atoms. In general, default settings of the BAND program were used. The Self-Consistent Field convergence criterion was set at 10^{-6} Hartree atomic units, while the geometrical optimization criterion was set at 10^{-2} Hartree per nanometer.

A (4x4) MoS_2 unit cell was employed, in the form of a stripe with periodicity in one direction. The stripe contains both an S-type edge and an Mo-type edge. The S-type edge was kept fully covered in all calculations (2 S edge atoms per Mo edge atom). The length of the unit cell was kept at the value optimized for 50%S coverage: 1.248 nm. For the calculations where the gold support was included, the Au(111) surface was modeled by a 2 layer slab with a lattice parameter commensurate with the MoS_2 stripe. The S-Mo-S-Au-Au stacking was chosen as A-B-A-B-C, with a S-Au layer spacing of 0.442 nm. The number of k points chosen for sampling the Brillouin zone was 3 throughout.

Transition states were located as follows: for a chosen reaction coordinate (usually an interatomic distance) total energies were computed for a range of fixed values (while optimizing all other degrees of freedom). For the structure of highest energy a partial hessian was calculated, including atoms at or close to the reaction site. The most negative eigenvalue of this partial hessian was used to locate the saddle point. In most cases the search had to be restarted several times by recomputing the partial hessian

on the structure with the smallest gradient found so far. It was checked that the partial hessian of the final structure had precisely one negative eigenvalue.

The reaction energies (ΔE_r) used in the computation of phase diagrams were calculated per unit cell as:

$$\Delta E_r = E_{MoS_2,S_xH_y} - E_{MoS_2} - xE_{H_2S} - (\tfrac{1}{2}y - x)E_{H_2} \quad (3.4)$$

In Equation 3.4, E_x denotes the total electronic energy obtained from DFT for the respective structure. In order to calculate the free energy of an edge structure, entropic corrections need to be applied:

$$\Delta\mu_S = RTln(\tfrac{P_{H_2S}}{P_{H_2}}) - T(S^o_{H_2S} - S^o_{H_2}) \quad (3.5)$$

$$\Delta\mu_H = \tfrac{1}{2}(RTln(P_{H_2}) - TS^o_{H_2}) \quad (3.6)$$

The standard entropies (S^o_x) in these equations were obtained from thermodynamic tables[33]. Using the entropic corrections, one can compute the free energy change involved in a reaction as:

$$\Delta G_r = \Delta E_r - x\Delta\mu_S - y\Delta\mu_H \quad (3.7)$$

The structure with the lowest free energy per unit cell at a particular combination of $\Delta\mu_S$ and $\Delta\mu_H$ values will be the phase present under those conditions. Note that with this definition of the free energy, we assume that all solid phases have zero entropy and that there is no change in heat capacity during the reaction.

To model the adsorption of CH_3SH, we first calculated the adsorption energy:

$$\Delta E_{ads} = E_{MoS_2,S_xH_y,MT_z} - E_{MoS_2,S_xH_y} - zE_{MT} \quad (3.8)$$

In Equation 3.8, MT corresponds to CH_3SH. The thermodynamic stability of the adsorbed CH_3SH structure was calculated as its formation free energy with respect to the most stable phase in the absence of CH_3SH adsorption:

$$\Delta G_f = \Delta E_{ads} - z\Delta\mu_{MT} + \Delta G_{r-MoS_2,S_xH_y} - \Delta G_{r-MoS_2,S_nH_m} \quad (3.9)$$

$$\Delta\mu_{MT} = RTln(P_{MT}) - TS^o_{MT} \quad (3.10)$$

In Equation 3.9, MoS_2,S_nH_m is the most stable structure in the absence of CH_3SH adsorption.

Finally, we performed a kinetic analysis using the free energy barriers that link the reaction intermediates. Entropic corrections were again applied using equations 3.5, 3.6 and 3.10. Rate constants were calculated from the free energy barriers (ΔG_a) using transition state theory:

$$k = \frac{k_B T}{h} e^{\frac{-\Delta G_a}{k_B T}} \tag{3.11}$$

Here, we assume that there is no communication between adjacent unit cells. By incorporating the pressure effect on the free energy in the calculation of *k*, all rates take the form:

$$r_n = k_n \theta_n \tag{3.12}$$

When the reaction reaches steady state, all coverages will be fixed. Thus, we obtain a set of linear equations, shown here for the example of an intermediate with two links to other intermediates.

$$\frac{d\theta_n}{dt} = k_{n-1}\theta_{n-1} + k_{-n}\theta_{n+1} - (k_{-(n-1)} + k_n)\theta_n = 0 \tag{3.13}$$

By solving this set of equations, one obtains the steady state coverage of the various intermediates.

References

[1] R.P. Silvy, Refining catalyst market begins to recover in 2010, Oil Gas J. 108 (2010) 40–43.

[2] M.A. Fahim, T.A. Al-Sahhaf, A. Elkilani, Fundamentals of Petroleum Refining, Elsevier, Oxford, 2010.

[3] I.G. Farbenindustrie A.G., British Patent 315439, 1928.

[4] S. Helveg, J. Lauritsen, E. Laegsgaard, I. Stensgaard, J. Norskov, B. Clausen, H. Topsoe, F. Besenbacher, Atomic-scale structure of single-layer MoS2 nanoclusters, Phys. Rev. Lett. 84 (2000) 951–4.

[5] L.P. Hansen, Q.M. Ramasse, C. Kisielowski, M. Brorson, E. Johnson, H. Topsøe, S. Helveg, Atomic-scale edge structures on industrial-style MoS 2 nanocatalysts, Angew. Chemie - Int. Ed. 50 (2011) 10153–10156.

[6] Y. Zhu, Q.M. Ramasse, M. Brorson, P.G. Moses, L.P. Hansen, C.F. Kisielowski, S. Helveg, Visualizing the stoichiometry of industrial-style Co-Mo-S catalysts with single-atom sensitivity, Angew. Chemie - Int. Ed. 53 (2014) 10723–10727.

[7] J. Kibsgaard, J. V. Lauritsen, E. Lægsgaard, B.S. Clausen, H. Topsøe, F. Besenbacher, Cluster-support interactions and morphology of MoS2 nanoclusters in a graphite-supported hydrotreating model catalyst, J. Am. Chem. Soc. 128 (2006) 13950–13958.

[8] J. Kibsgaard, B.S. Clausen, H. Topsøe, E. Lægsgaard, J. V. Lauritsen, F. Besenbacher, Scanning tunneling microscopy studies of TiO2-supported hydrotreating catalysts: Anisotropic particle shapes by edge-specific MoS2-support bonding, J. Catal. 263 (2009) 98–103.

[9] A. Tuxen, J. Kibsgaard, H. Gøbel, E. Lægsgaard, H. Topsøe, J. V. Lauritsen, F. Besenbacher, Size threshold in the dibenzothiophene adsorption on MoS2 nanoclusters, ACS Nano. 4 (2010) 4677–4682.

[10] M. Brorson, A. Carlsson, H. Topsøe, The morphology of MoS2, WS2, Co-Mo-S, Ni-Mo-S and Ni-W-S nanoclusters in hydrodesulfurization catalysts revealed by HAADF-STEM, Catal. Today. 123 (2007) 31–36.

[11] J. V. Lauritsen, M. Nyberg, J.K. Nørskov, B.S. Clausen, H. Topsøe, E. Lægsgaard, F. Besenbacher, Hydrodesulfurization reaction pathways on MoS2 nanoclusters revealed by scanning tunneling microscopy, J. Catal. 224 (2004) 94–106.

[12] A.K. Tuxen, H.G. Füchtbauer, B. Temel, B. Hinnemann, H. Topsoe, K.G. Knudsen, F. Besenbacher, J. V. Lauritsen, Atomic-scale insight into adsorption of sterically hindered dibenzothiophenes on MoS2 and Co-Mo-S hydrotreating catalysts, J. Catal. 295 (2012) 146–154.

[13] P.G. Moses, B. Hinnemann, H. Topsøe, J.K. Nørskov, The hydrogenation and direct desulfurization reaction pathway in thiophene hydrodesulfurization over MoS2 catalysts at realistic conditions: A density functional study, J. Catal. 248 (2007) 188–203.

[14] P.G. Moses, B. Hinnemann, H. Topsøe, J.K. Nørskov, The effect of Co-promotion on MoS2 catalysts for hydrodesulfurization of thiophene: A density functional study, J. Catal. 268 (2009) 201–208.

[15] J. V. Lauritsen, M. V. Bollinger, E. Lægsgaard, K.W. Jacobsen, J.K. Nørskov, B.S.

Clausen, H. Topsøe, F. Besenbacher, Atomic-scale insight into structure and morphology changes of MoS2 nanoclusters in hydrotreating catalysts, J. Catal. 221 (2004) 510–522.
[16] B. Baubet, M. Girleanu, A.S. Gay, A.L. Taleb, M. Moreaud, F. Wahl, V. Delattre, E. Devers, A. Hugon, O. Ersen, P. Afanasiev, P. Raybaud, Quantitative Two-Dimensional (2D) Morphology-Selectivity Relationship of CoMoS Nanolayers: A Combined High-Resolution High-Angle Annular Dark Field Scanning Transmission Electron Microscopy (HR HAADF-STEM) and Density Functional Theory (DFT) Study, ACS Catal. 6 (2016) 1081–1092.
[17] M. V. Bollinger, K.W. Jacobsen, J.K. Nørskov, Atomic and electronic structure of MoS2 nanoparticles, Phys. Rev. B. 67 (2003) 085410.
[18] P.Y. Prodhomme, P. Raybaud, H. Toulhoat, Free-energy profiles along reduction pathways of MoS2 M-edge and S-edge by dihydrogen: A first-principles study, J. Catal. 280 (2011) 178–195.
[19] S. Cristol, J.F. Paul, E. Payen, D. Bougeard, S. Clémendot, F. Hutschka, Theoretical Study of the MoS2(100) Surface: A Chemical Potential Analysis of Sulfur and Hydrogen Coverage, J. Phys. Chem. B. 106 (2002) 5659–5667.
[20] N. Dinter, M. Rusanen, P. Raybaud, S. Kasztelan, H. Toulhoat, Temperature-programed reduction of unpromoted MoS 2 -based hydrodesulfurization catalysts : Experiments and kinetic modeling from first principles, J. Catal. 267 (2009) 67–77.
[21] A. Bruix, H.G. Füchtbauer, A.K. Tuxen, A.S. Walton, M. Andersen, S. Porsgaard, F. Besenbacher, B. Hammer, J. V Lauritsen, In Situ Detection of Active Edge Sites in Single-Layer MoS 2 Catalysts, ACS Nano. 9 (2015) 9322–9330.
[22] C.T. Herbschleb, P.C. van der Tuijn, S.B. Roobol, V. Navarro, J.W. Bakker, Q. Liu, D. Stoltz, M.E. Cañas-Ventura, G. Verdoes, M.A. van Spronsen, M. Bergman, L. Crama, I. Taminiau, A. Ofitserov, G.J.C. van Baarle, J.W.M. Frenken, The ReactorSTM: atomically resolved scanning tunneling microscopy under high-pressure, high-temperature catalytic reaction conditions., Rev. Sci. Instrum. 85 (2014) 083703.
[23] H. Häkkinen, The gold–sulfur interface at the nanoscale, Nat. Chem. 4 (2012) 443–455.
[24] H.G. Füchtbauer, A.K. Tuxen, Z. Li, H. Topsøe, J. V. Lauritsen, F. Besenbacher, Morphology and atomic-scale structure of MoS2 nanoclusters synthesized with different sulfiding agents, Top. Catal. 57 (2014) 207–214.
[25] Y. V. Joshi, P. Ghosh, P.S. Venkataraman, W.N. Delgass, K.T. Thomson, Electronic descriptors for the adsorption energies of sulfur-containing molecules on co/mos2, using dft calculations, J. Phys. Chem. C. 113 (2009) 9698–9709.
[26] BAND2014, (2014). http://scm.com.
[27] G. Te Velde, E.J. Baerends, Precise density-functional method for periodic structures, Phys. Rev. B. 44 (1991) 7888–7903.
[28] G. Wiesenekker, E.J. Baerends, Quadratic integration over the three-dimensional Brillouin zone, J. Phys. Condens. Matter. 3 (1991) 6721–6742.
[29] M. Franchini, P.H.T. Philipsen, L. Visscher, The becke fuzzy cells integration scheme in the amsterdam density functional program suite, J. Comput. Chem.

34 (2013) 1819–1827.
[30] M. Franchini, P.H.T. Philipsen, E. Van Lenthe, L. Visscher, Accurate Coulomb potentials for periodic and molecular systems through density fitting, J. Chem. Theory Comput. 10 (2014) 1994–2004.
[31] J.P. Perdew, K. Burke, M. Ernzerhof, Generalized Gradient Approximation Made Simple, Phys. Rev. Lett. 77 (1996) 3865–3868.
[32] S. Grimme, S. Ehrlich, L. Goerigk, Effect of damping function in dispersion corrected Density Functional Theory, J. Comput. Chem. 32 (2010) 1456–1465.
[33] NIST, Computational Chemistry Comparison and Benchmark Database, (2016). http://cccbdb.nist.gov/.

Chapter 3 - Supporting information

In situ observations of an active MoS_2 hydrodesulfurization model catalyst

3.5 Appearance of MoS_2 edge structures in scanning tunneling microscopy

The electrons that make up the tunneling current in scanning tunneling microscopy (STM) originate from states close to the Fermi level. As the local density of these states is usually not evenly distributed over the atoms of the sample, the appearance of structures in STM often does not directly reflect the atomic structure. The edges of MoS_2 islands present a particularly pronounced case of such a discrepancy. Hence, in order to interpret the STM images properly, it is necessary to compare them to calculations of the local density of states using density functional theory (DFT). STM images are usually modeled as contours of equal values of the local density of states (LDOS) around the Fermi level. The LDOS around the Fermi level is typically obtained by summation over all LDOS contributions at and around the Fermi level with a Gaussian weighting (Tersoff-Hamann method[1,2]). Because the width of the Gaussian is somewhat arbitrary, we have chosen instead to sum over the LDOS from the Fermi level to the applied sample bias (-0.3 V), which does not require any other parameters. The additional benefit of this method is that the states further from the Fermi level are taken into account more appropriately.

Figure 3.6 shows simulated STM images of the 100%S, 50%S and 50%S-50%H structures. From Figure 3.6a, it is clear that the LDOS at the edge of the particle strongly deviates from the atomic arrangement for the 100%S structure. Hence, in the STM images for this structure the edge S atoms will appear not to follow the lattice of the particles' basal plane, even though in reality they do. The 50%S structure shows a similar discrepancy between atomic structure and LDOS (see Figure 3.6b). However, a small fraction of the LDOS remains located around the S edge atoms, resulting in the red protrusions in the image. For a tip with a finite size however, the bright protrusions will dominate the image. Hence, the edge atoms will appear to be in registry with the basal plane S atoms.

For the case of the 50%S-50%H structure in Figure 3.6c, the situation is less clear. Some of the protrusions on the edge are in registry with the basal plane, while others are not. At elevated temperatures, the H-atoms on the edge will diffuse at high rates, because the diffusion barrier is only 0.56 eV (obtained for unsupported MoS_2). Therefore, a time average of Figure 3.6c would be observed in STM. In such a time average, the brightest protrusion will typically dominate the observed structure due to the exponential character of the tunneling current as a function of tip-surface distance. In the case of the 50%S-50%H structure, the brightest protrusion appears in registry with the basal plane. Therefore, the 50%S-50%H structure will appear similar to the 50%S structure, although with significantly less corrugation along the edge.

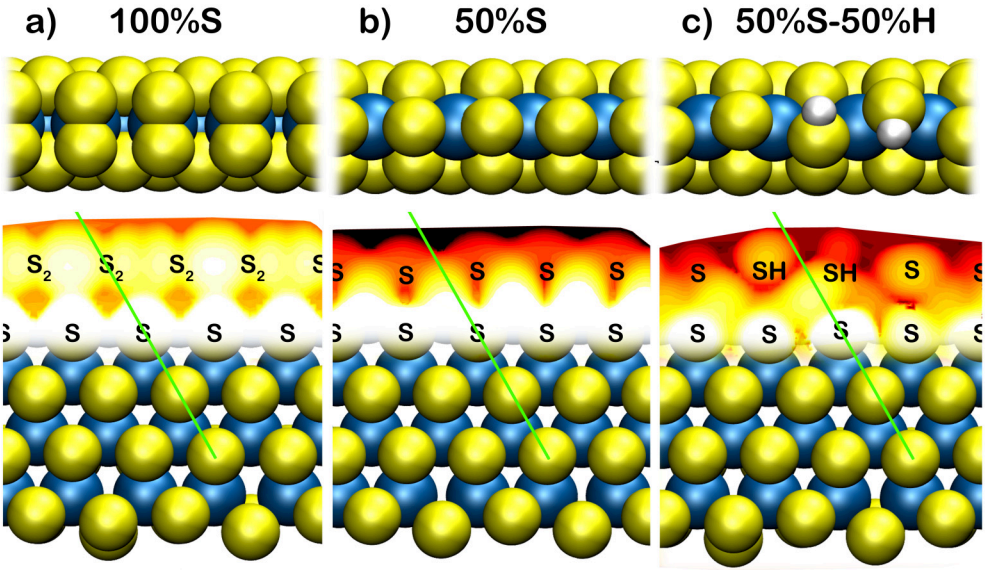

Figure 3.6: Simulated STM images of a) the 100%S structure, b) the 50%S structure and c) the 50%S-50%H structure, for U_s = -0.3 V and at a countour value of $1x10^{-5}$ AU. The green lines facilitate comparison of the registry of the edge protrusions with respect to the basal plane S atoms.

As noted in the main text, Bruix *et al.* obtained a different result for the appearance of the 50%S edge[3]. We identify two possible explanations. First, they used the Tersoff-Hamann method for the calculation of the LDOS around the Fermi level. As pointed out by Bollinger *et al.*, who found a result in agreement with ours, the choice of the Gaussian width is very sensitive in the particular case of MoS_2 due to its semiconducting properties[2]. Hence, the discrepancy between the different authors may be explained due to a different choice for this parameter. A second explanation may be a different placement of MoS_2 on the Au support. If we remove the gold in our calculations, the registry shift in the 50%S structure vanishes. Hence, the details of the MoS_2-Au interaction may be decisive in the obtained results.

3.6 Effect of the Au support on the relative stability of MoS_2 edge structures

To assess the influence of the Au(111) support on the relative stability of MoS_2 edge structures, phase diagrams were computed with and without Au(111) support, as shown in Figure 3.7. Clearly, gold-supported MoS_2 favors higher edge sulfur coverage than its unsupported counterpart. Nonetheless, Au(111) is considered a weakly interacting support[4] since it does not significantly change the edge structures. In contrast, oxide supports like TiO_2 and Al_2O_3 are thought to make oxygen linkages at the particle edges[4–6].

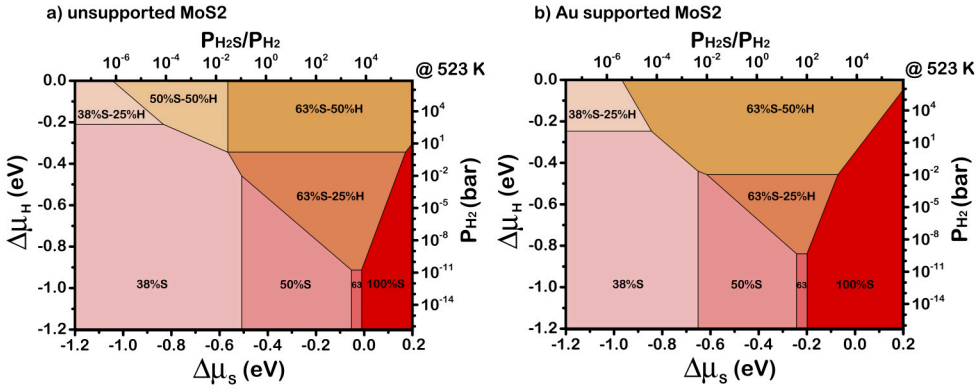

Figure 3.7: *Ab initio* thermodynamics phase diagrams of the MoS_2 edge structure in H_2/H_2S mixtures. a) Unsupported MoS_2. b) Au-supported MoS_2.

3.7 Comparison of the calculations to literature

To establish the validity of our calculations, we compared our results to those reported in the literature. We note that in all previously published phase diagrams, the sulfur chemical potential was referenced against various sulfur structures. This leads to a somewhat arbitrary offset with respect to our chemical potential. Based on the conversion to pressure (ratio) at specific temperatures mentioned in the respective articles, we estimate this offset to be -0.1 eV for Bollinger *et al.*[2] and Lauritsen *et al.*[7], -0.23 eV for Prodhomme *et al.*[8], and -4.15 eV for Cristol *et al.*[9]. Using these offsets, we constructed the comparison in Table 3.1. From these results, it is clear that the relative energies of various edge structures are reproduced relatively well, independent of the differences in methods or unit cell.

Table 3.1: Relative stability of 50%S and 100%S structures

Authors	$\Delta\mu_{H\text{-}50S\searrow 50S\text{-}50H}$ unsupported	$\Delta\mu_{H\text{-}50S\searrow 50S\text{-}50H}$ Au supported	$\Delta\mu_{S\text{-}50S\searrow 100S}$ unsupported	$\Delta\mu_{S\text{-}50S\searrow 100S}$ Au supported
Present	-0.37 eV	-0.30 eV	-0.02 eV	-0.21 eV
Bollinger *et al.*[2]	-0.30 eV		-0.11 eV	
Lauritsen *et al.*[7]		-0.30 eV		-0.33 eV
Prodhomme *et al.*[8]	-0.35 eV			
Cristol *et al.*[9]			0.01 eV	

3.8 CH_3SH adsorption on MoS_2

The adsorption energy of CH_3SH on Au-supported MoS_2 was calculated for a coverage of 1 molecule per 4 Mo edge atoms. For the calculation of the free energy of adsorption, entropic contributions were included using the reaction conditions in the

STM experiment (P_{CH3SH} = 0.1 bar, P_{H2S} = ~0.001 bar, P_{H2} = 0.9 bar, 523 K). The formation energy of the adsorption structures was referenced against the most stable structure in the absence of CH_3SH, namely 63%S-50%H.

Table 3.2: Energetics of CH_3SH adsorption on MoS_2

Structure	E_{ads}	ΔG_{ads}	ΔG_{form}
37%S	-1.62 eV	-0.13 eV	-0.08 eV
50%S-50%H	-1.28 eV	0.21 eV	0.44 eV
87%S	-0.46 eV	1.03 eV	2.90 eV

References

[1] J. Tersoff, D.R. Hamann, Theory of the scanning tunneling microscope, Phys. Rev. B. 31 (1985) 805–813.

[2] M. V. Bollinger, K.W. Jacobsen, J.K. Nørskov, Atomic and electronic structure of MoS2 nanoparticles, Phys. Rev. B. 67 (2003) 085410.

[3] A. Bruix, H.G. Füchtbauer, A.K. Tuxen, A.S. Walton, M. Andersen, S. Porsgaard, F. Besenbacher, B. Hammer, J. V Lauritsen, In Situ Detection of Active Edge Sites in Single-Layer MoS 2 Catalysts, ACS Nano. 9 (2015) 9322–9330.

[4] A.S. Walton, J. V. Lauritsen, H. Topsøe, F. Besenbacher, MoS2 nanoparticle morphologies in hydrodesulfurization catalysis studied by scanning tunneling microscopy, J. Catal. 308 (2013) 306–318. doi:10.1016/j.jcat.2013.08.017.

[5] B. Hinnemann, J.K. Nørskov, H. Topsøe, A density functional study of the chemical differences between Type I and Type II MoS2-based structures in hydrotreating catalysts., J. Phys. Chem. B. 109 (2005) 2245–53.

[6] N. Topsøe, H. Topsøe, FTIR studies of Mo/Al2O3 based catalysis. I.Morphology and Structure of Calcined and Sulfided Catalysts, J. Catal. 139 (1993) 631 – 640.

[7] J. V. Lauritsen, M. V. Bollinger, E. Lægsgaard, K.W. Jacobsen, J.K. Nørskov, B.S. Clausen, H. Topsøe, F. Besenbacher, Atomic-scale insight into structure and morphology changes of MoS2 nanoclusters in hydrotreating catalysts, J. Catal. 221 (2004) 510–522.

[8] P.Y. Prodhomme, P. Raybaud, H. Toulhoat, Free-energy profiles along reduction pathways of MoS2 M-edge and S-edge by dihydrogen: A first-principles study, J. Catal. 280 (2011) 178–195.

[9] S. Cristol, J.F. Paul, E. Payen, D. Bougeard, S. Clémendot, F. Hutschka, Theoretical Study of the MoS2(100) Surface: A Chemical Potential Analysis of Sulfur and Hydrogen Coverage, J. Phys. Chem. B. 106 (2002) 5659–5667.